ELSEVIER

Journal of Structural Geology 29 (2007) 256–272

JOURNAL OF STRUCTURAL GEOLOGY

www.elsevier.com/locate/jsg

Constraints on deformation path from finite strain gradients

Eric Horsman*, Basil Tikoff

Department of Geology and Geophysics, University of Wisconsin-Madison, 1215 W Dayton Street, Madison, WI 53706, USA

Received 13 January 2006; received in revised form 9 September 2006; accepted 10 September 2006
Available online 2 November 2006

Abstract

We present a methodology for analyzing finite strain gradients in high-strain zones in order to place constraints on the zone's possible deformation path. To accomplish this, the high-strain zone is divided into several sub-zones, within each of which finite strain is described by a single ellipsoid. Based on knowledge of the spatial and temporal evolution of deformation, strain observed in less deformed sub-zones is then mathematically removed from more deformed sub-zones to calculate incremental finite strains. The mean kinematic vorticity number of each of these increments must be constant if deformation was steady-state. We use the methodology to analyze two natural examples of high-strain zones at different scales. Both natural examples have non-steady-state likely deformation paths, which may be a common characteristic of high-strain zones. Although results of the methodology are not unique, identification of likely paths considerably narrows the range of possible deformation paths. Consequently, useful kinematic information can be extracted from finite strain data even in instances where the detailed spatial and temporal evolution of a high-strain zone cannot be determined conclusively.

Keywords: Deformation; Finite strain analysis; Kinematics; Shear zone

1. Introduction

High-strain zones commonly display gradients in finite strain that can provide insight into how rock deforms. For example, it is possible to calculate zone offset amount from finite strain gradients (e.g. Simpson, 1985; Zhang and Hynes, 1995), which allows tectonic reconstructions (e.g. Giorgis et al., 2005). In some instances, inferences about the kinematic history or deformation path of the zone can be drawn from finite strain gradients. The orientation and magnitude of finite strain with respect to the high-strain zone boundary, for example, can constrain the kinematics of the zone if steady-state deformation is assumed (e.g. Tikoff and Fossen, 1995; Bailey and Eyster, 2003; Giorgis et al., 2004). For the purposes of this article we refer to the term *steady-state* in the context of *geometric steady-state*, indicating that the orientation of infinitesimal straining remains fixed during deformation (e.g. Bobyarchick, 1986) but that the bulk strain rate may vary. This term is distinct from *kinematic steady-state* deformation, which refers to the situation where infinitesimal straining axes remain fixed and the bulk strain rate remains constant (e.g. *steady flow* of Malvern, 1969, p. 143 and Furbish, 1997, pp. 168–9; *steady-state deformation* of Provost et al., 2004). All kinematic steady-state deformations are necessarily geometric steady-state.

Geological deformation is often assumed to be kinematic steady-state principally because it is mathematically simpler to consider than non-steady-state deformation. The problem in evaluating this assumption stems from the difficulty inherent in extracting information about deformation path from the rock record (Means, 1976, pp. 25–30). In particular, a theoretically infinite variety of deformation paths may lead to the same finite strain (e.g. Elliott, 1972; Passchier, 1988; Jiang and White, 1995; Fossen and Tikoff, 1997). This non-uniqueness has limited progress in our quantitative understanding of high-strain zones.

We hypothesize that finite strain gradients can be used to corroborate or falsify the assumption of geometric steady-state

* Corresponding author. Tel.: +1 608 262 9252.
E-mail address: eric@geology.wisc.edu (E. Horsman).

0191-8141/$ - see front matter © 2006 Elsevier Ltd. All rights reserved.
doi:10.1016/j.jsg.2006.09.003

deformation. Our approach is to mathematically remove strain observed in low-strain domains from that observed higher-strain domains. This approach allows characterization of a series of incremental strain values (Fig. 1). If incremental finite strains are all consistent with a single kinematic framework then, as a first-order approximation, steady-state history can be reasonably assumed. Further, with application of simple well-established models of high-strain zone growth (e.g. Types I–III of Hull, 1988; Mitra, 1991; Means, 1995), finite strain gradients can be analyzed and interpreted in order to provide constraints on the most likely deformation path of high-strain zones. By considering the spatial and temporal evolution of strain accumulation, we can place constraints on the kinematic history of a deformed zone. In this contribution, we apply the approach to two different high-strain zones reported in the literature, determine if the deformation was steady-state and provide a reasonable interpretation for the kinematic evolution of the zones.

2. Procedure

By understanding the spatial and temporal distribution of straining in high-strain zones, the kinematic history recorded in the rocks can be studied by mathematically removing strain fields. Although a universal analysis procedure cannot be laid out, the goals are straightforward to describe. (1) The geometric evolution of the high-strain zone is characterized. Observations of fabric symmetry and overprinting relationships may be useful in distinguishing between various possible deformation geometry histories. (2) The zone is subdivided into component sub-zones, each of which has roughly homogeneous finite strain magnitude, shape, and orientation. (3) Finite strain is measured in each sub-zone. Note that simple measurement of fabric type (e.g. $S > L$) and fabric orientation is necessary but insufficient for this analysis. Rather, some measure of finite strain is necessary so that deformation can be studied quantitatively rather than qualitatively. (4) Incremental strains are calculated from the observed finite strain. Mathematical methods for calculating these incremental strains vary slightly based on the spatial and temporal evolution of straining within the high-strain zone. (5) The mean kinematic vorticity number of each increment of strain is calculated. (6) Finally, constraints are placed on the high-strain zone's deformation path based on consideration of the collected and calculated information.

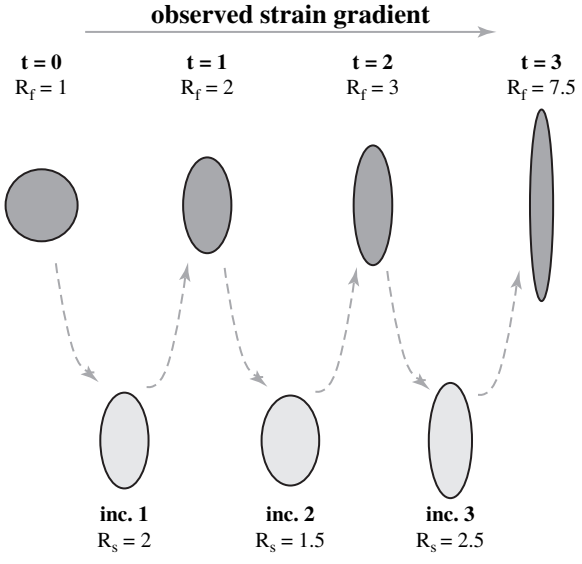

Fig. 1. Incremental strains can be calculated from a finite strain gradient. In this two-dimensional pure shear example, finite strain ellipses (in dark gray) exhibit a strain gradient (R_f increases from left to right). Incremental strain ellipses (in light gray) can be calculated and describe the amount of deformation (R_s) between observed finite strains. Deformation path in this case is geometric steady-state (consistently pure shear, but the bulk strain rate may have varied).

The following more detailed description of this analysis procedure relies on terminology commonly used to describe the spatial and temporal distribution of finite straining within high-strain zones. First, to distinguish between observed deformation and the processes through which the deformation in produced, we follow previous authors (e.g. Ramberg, 1975; Lister and Williams, 1983) and append the suffix *-ing* to terms referring to processes. For example, simple shear kinematics produce finite strain through progressive simple shearing. Additionally, we use separate terms to describe how the velocity field varies spatially and how at a particular point in space the field is decomposed into different components (e.g. simple shearing and pure shearing). We use the term *partitioning* to describe the spatial variation of the velocity field. Additionally, different parts of a deforming region may simultaneously accumulate finite strain at different rates and with different divisions of the velocity field into components like shear-induced vorticity and spin (Lister and Williams, 1983). We refer to this process as *decomposition*. Partitioning and decomposition of the velocity field into straining components have been interpreted from field observations of high-strain zones (e.g. Tikoff and Teyssier, 1994; Jones and Tanner, 1995; Goodwin and Williams, 1996; Holdsworth et al., 2002; MacInnes and White, 2004) and are probably an important mechanism for progressive deformation of mechanically heterogeneous rocks (e.g. Treagus et al., 1983; Treagus, 1988, 1993; Ishii, 1992; Simpson and DePaor, 1993; Jiang and White, 1995; Goodwin and Tikoff, 2002).

2.1. System characterization

Prior to any quantitative consideration of a high-strain zone's deformation path, the geometrical structure of the zone must be investigated. Toward this end, we refer to the temporal divisions of finite strain as *increments* and to the spatial divisions as *sub-zones*.

Once the broad boundaries of the high-strain zone have been recognized, the zone is divided up into sub-zones, each of which records a roughly homogeneous finite strain magnitude and orientation. In addition to determining the finite strain in each sub-zone, the geometry and dimensions of these sub-zones should be determined as carefully as possible.

Quantifying the finite strain in each sub-zone requires the establishment of a coordinate system. Subsequent analysis is almost invariably simplified if coordinate axes are fixed parallel to the boundaries of the high-strain zone (see Section 2.2). The finite strain in each sub-zone is now quantified with respect to the imposed coordinate system. Observed finite strain within each sub-zone should be described with a second-rank tensor. All of these tensors should be in the same coordinate system.

Note that identification of sub-zones depends on the scale at which the increments of strain are to be analyzed. For example, during analysis of a kilometer-wide high-strain zone, heterogeneous deformation at the meter scale or smaller may be insignificant when considering the bulk deformation. Specific circumstances may require special consideration. Knowledge of wallrock deformation history is also important. Traditional mathematical strain analysis of shear zones (e.g. Ramsay and Graham, 1970; Ramsay, 1980) assumes that wallrock remains undeformed; strain is assumed to accumulate only in the shear zone. While this simplification may be technically inaccurate in some cases (e.g. Jones et al., 1997), it may be a reasonable approximation in other cases (e.g. Ramsay and Allison, 1979). One particularly important consequence of assuming that wallrock remains undeformed is that strain compatibility problems arise unless the high-strain zone deforms exclusively through simple shearing (Ramsay, 1980; Robin and Cruden, 1994). Calculating the bulk strain accommodated by a high-strain zone with heterogeneous non-simple shear kinematics (i.e. when strain incompatibility exists) can only be accomplished in cases where both discrete and distributed components of deformation can be thoroughly characterized (Horsman and Tikoff, 2005).

2.2. Geometric evolution of high-strain zones

High-strain zones can change geometry and volume as time and deformation progress (Means, 1995). Understanding this evolution is essential to constraining the zone's deformation path because strain and fabric formed during early phases of deformation can be modified or entirely overprinted during subsequent phases of deformation. To simplify our presentation, terminology used to describe such evolution is described here using three end-member geometries: constant-volume deformation, and localizing and delocalizing deformations (both of which are changing-volume deformations in the sense that the volume of deforming material varies as high-strain zone boundaries migrate through the material). It is important to note that the geometric evolution of a high-strain zone can be considerably more complicated than the end-member possibilities considered in our examples below. More complicated natural geometric evolution histories can, however, be analyzed using our methodology provided the zone's evolution can be established. In the Section 6, we will consider limitations of our methodology pertinent to analyzing complicated deformation histories. For the purposes of describing high-strain zone geometric evolution, the following discussion assumes planar zone boundaries and monoclinic symmetry.

2.2.1. Constant-volume deformation

Constant-volume deformation involves high-strain zone boundaries that remain fixed in a material reference frame but may migrate within a spatial reference frame (Type III shear zone of Hull, 1988; Mitra, 1991; Means, 1995). In Fig. 2, the constant-volume example shows a case in which zone boundaries remain fixed in both material and spatial

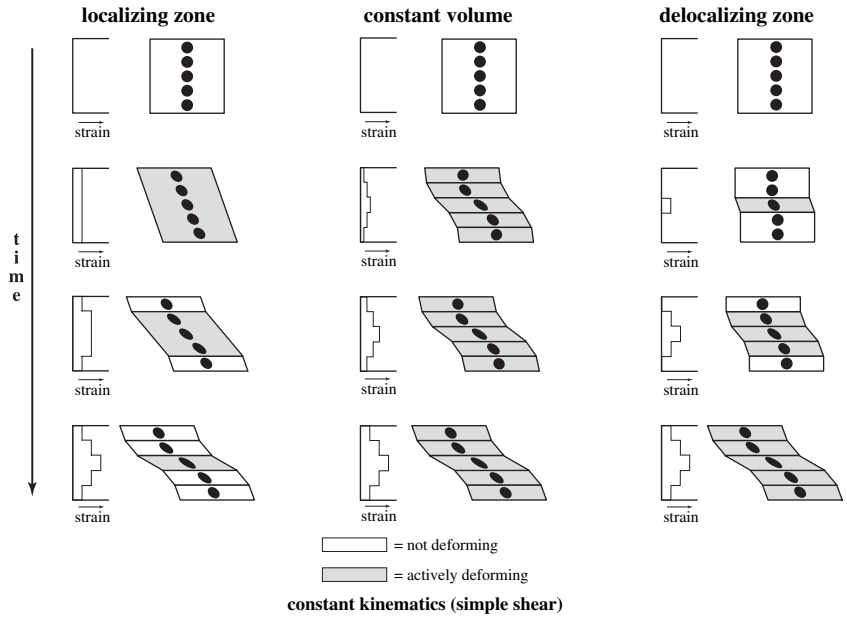

Fig. 2. Examples of the evolution of straining in three end-member types of high-strain zones: localizing, constant-volume, and delocalizing. All examples in this case involve simple shear kinematics and result in the same final observed strain geometry. Shaded regions in the block diagrams and the strain profiles indicate active deformation. Schematic cumulative strain profiles are shown for each zone at four stages of progressive deformation. These strain profiles describe the variation in strain one would observe across the high-strain zone at that increment of time.

reference frames throughout deformation. This example would still be a constant-volume deformation if the outer edges of the zone moved closer to one another during deformation as long as this shortening was balanced by extension in another direction.

Strain need not be homogeneous within a constant-volume high-strain zone, as is shown in Fig. 2. Analysis of constant-volume high-strain zones is, however, limited by the fact that strain within each sub-zone must be considered independently. Different finite strain observed in each sub-zone can be interpreted to be the result of either steady-state or non-steady-state heterogeneous partitioning of pure shearing and simple shearing components of the bulk velocity field throughout deformation history. It is impossible to distinguish between these possibilities using solely finite strain evidence. Consequently, analysis of constant-volume deformation zones provides no conclusive information about the evolution of bulk high-strain zone deformation path, and we instead focus on changing-volume deformations in the analyses presented in this paper.

2.2.2. Changing-volume deformation

Many high-strain zones have boundaries that migrate with time in both the material and spatial reference frames (Fig. 2). Migration of zone boundaries in the material reference frame produces changes in the volume of actively deforming rock. We use the term *localization* to describe a zone whose boundaries migrate through material and grow closer together during deformation, progressively localizing deformation and decreasing the volume of actively deforming material (e.g. White et al., 1980; Passchier, 1986; Wojtal and Mitra, 1988; West and Hubbard, 1997; Type II shear zone of Means, 1984, 1995; Hull, 1988; Mitra, 1991). We use the term *delocalizing* to describe the opposite case in which a high-strain zone becomes less localized over time and the volume of actively deforming material increases (e.g. Wojtal and Mitra, 1988; Aoya and Wallis, 2003; Type I shear zone of Means, 1984, 1995; Hull, 1988; Mitra, 1991). High-strain zones here classified as localizing and delocalizing can also be described with the genetic terms *weakening* and *hardening*, respectively. However, because we are concerned only with the description of high-strain zone geometry, we favor the use of descriptive rather than genetic terms.

2.3. Calculation of incremental finite strains

The general procedure for calculation of incremental finite strains from a thoroughly characterized finite strain gradient is schematically illustrated in Fig. 3. For the purpose of demonstrating the methodology, Fig. 3a shows a forward deformation in which three increments of finite strain are superposed sequentially to produce a finite strain gradient. Each increment affects a smaller area than the previous increment; this is a localizing deformation. Analysis of natural strain gradients necessarily involves reciprocal deformation, in which observed finite strain gradients are mathematically undeformed. Fig. 3b shows the reciprocal deformation of the finite strain gradient produced by progressive localization as shown in Fig. 3a.

Specific analysis procedures vary for localizing and delocalizing high-strain zones but in general, analysis involves mathematical removal of finite strain observed in relatively little-deformed sub-zones from the finite strain observed in more deformed sub-zones. For the purposes of completeness, we also discuss mathematical analysis of constant-volume high-strain zones.

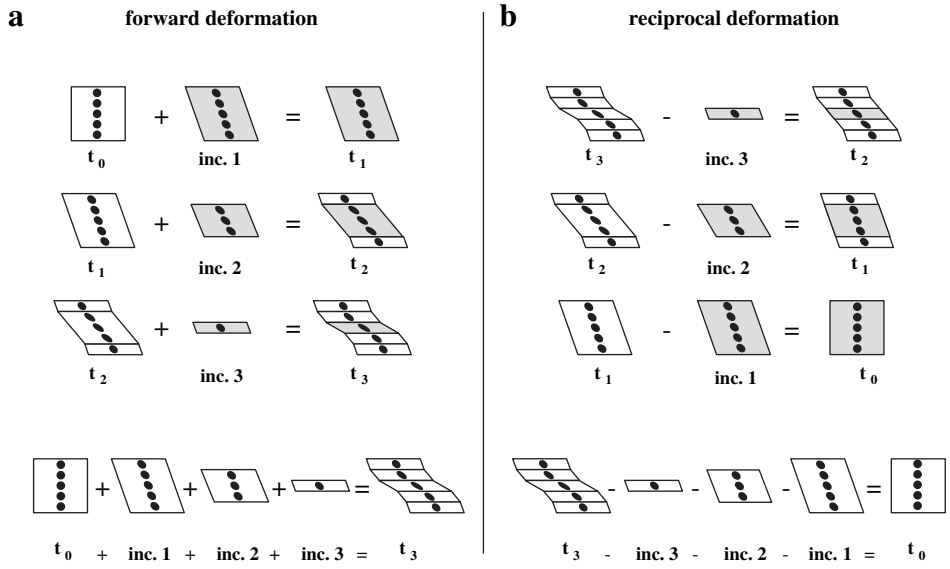

Fig. 3. Comparison of forward and reciprocal deformation. Analysis of deformation path in naturally deformed rocks necessarily involves reciprocal deformation. Straining regions are shown in gray. Inactive regions are shown in white. (a) Schematic representation of the geometric evolution of straining in a localizing two-dimensional simple shear high-strain zone. Strain accumulates in progressively more localized sub-zones. (b) Schematic representation of how strain can be removed from the observed high-strain zone to result in the initial condition.

2.4. Mathematical framework

We assume that the finite strain observed in a given sub-zone ($\mathbf{F}_n$) of a high-strain zone accumulated through the superposition of n increments of finite strain ($\mathbf{Z}_1$ through $\mathbf{Z}_n$):

$$\mathbf{F}_n = \mathbf{Z}_n \cdot \ldots \cdot \mathbf{Z}_2 \cdot \mathbf{Z}_1. \tag{1}$$

where $\mathbf{F}_n$ and $\mathbf{Z}_i$ ($1 \leq i \leq n$) are second-rank tensors in the same coordinate system. Superposition of finite strain increments (e.g. Fig. 3a) is mathematically manifested as matrix multiplication. The removal of strain increments, or reciprocal deformation (e.g. Fig. 3b), works similarly. This procedure assumes each increment of deformation accumulated during steady-state straining. The bulk deformation, however, may or may not be steady-state. The increments of finite strain $\mathbf{Z}_i$ will either all have the same mean kinematic vorticity number (see Section 2.5) in the case of steady-state deformation or, in the case of non-steady-state deformation, will have different mean kinematic vorticity numbers.

Calculation of incremental strain from a finite strain gradient depends on the geometric evolution of straining. Consequently, different procedures must be used to isolate strain increments in localizing and delocalizing high-strain zones. These different procedures result in different incremental tensors for localizing ($\mathbf{Z}_{L_i}$) and delocalizing ($\mathbf{Z}_{D_i}$) zones in some cases. Derivation and conceptual explanation of Eqs. (2) and (3) are given in Appendix A. In a localizing zone, isolation of increments follows a consistent pattern:

$$\mathbf{Z}_{L_1} = \mathbf{F}_1, \tag{2a}$$

$$\mathbf{Z}_{L_2} = \mathbf{F}_2 \cdot \mathbf{Z}_{L_1}^{-1}, \tag{2b}$$

$$\mathbf{Z}_{L_3} = \mathbf{F}_3 \cdot \mathbf{Z}_{L_1}^{-1} \cdot \mathbf{Z}_{L_2}^{-1}, \tag{2c}$$

…

$$\mathbf{Z}_{L_n} = \mathbf{F}_n \cdot \mathbf{Z}_{L_1}^{-1} \cdot \mathbf{Z}_{L_2}^{-1} \cdot \ldots \cdot \mathbf{Z}_{L_{n-1}}^{-1}. \tag{2d}$$

Isolation of increments in a delocalizing zone follows a different consistent pattern:

$$\mathbf{Z}_{D_n} = \mathbf{F}_1, \tag{3a}$$

$$\mathbf{Z}_{D_{n-1}} = \mathbf{Z}_{D_n}^{-1} \cdot \mathbf{F}_2, \tag{3b}$$

$$\mathbf{Z}_{D_{n-2}} = \mathbf{Z}_{D_{n-1}}^{-1} \cdot \mathbf{Z}_{D_n}^{-1} \cdot \mathbf{F}_3, \tag{3c}$$

…

$$\mathbf{Z}_{D_1} = \mathbf{Z}_{D_2}^{-1} \cdot \ldots \cdot \mathbf{Z}_{D_{n-1}}^{-1} \cdot \mathbf{Z}_{D_n}^{-1} \cdot \mathbf{F}_n. \tag{3d}$$

In contrast, analysis of deformation zones of constant-volume (neither localizing nor delocalizing over time) follows a different procedure. Strain within each sub-zone is assumed to have accumulated in a steady-state manner, but each of these component sub-zones may have had different kinematics due to partitioning (Fig. 1). As all of the sub-zones were active simultaneously throughout the bulk deformation, analysis of one sub-zone provides no information about the deformation history of other sub-zones, so each is analyzed independently from the others.

2.5. Incremental vorticity determination

Once incremental deformation tensors have been calculated, the mean kinematic vorticity number of each incremental deformation is calculated. The term *vorticity* is used to describe the instantaneous rate of rotation of material lines relative to the stretching of those lines in a viscous medium (Truesdell, 1954; Means et al., 1980; Passchier, 1986; Means, 1994). Vorticity analysis provides information on the kinematic framework in which a deformed rock acquired its fabric (Means et al., 1980; Passchier, 1988). For discussion on the assumptions inherent in geological vorticity analysis and limitations of such analysis see Jiang (1994), Jiang and White (1995) and Tikoff and Fossen (1995, 1999).

In geology, vorticity is often described as the ratio between the rate of simple shearing and the rate of pure shearing. Values for the kinematic vorticity number W therefore vary from $W = 0$ (pure shearing), through $W = 1$ (simple shearing), to $1 \leq W \leq \infty$ (super-simple shearing). Geologically meaningful values of the vorticity number generally range from $0 \leq W \leq 1$ for bulk deformation. Super-simple shearing arises from spinning flow regimes (Lister and Williams, 1983) and is therefore important in porphyroclasts and -blasts at the microstructural scale (e.g. Simpson and DePaor, 1993; Jiang and White, 1995) and perhaps at the outcrop scale (e.g. rotating veins and other competent domains; Jiang and White, 1995) but is probably rare at larger scales, with the notable exception of rotating crustal blocks.

Because of the mechanical heterogeneity of rocks and the finite nature of natural deformation, the true quantity of interest in kinematic analysis of deformed rocks is the average vorticity of a region over a period of time. This quantity incorporates the concepts of both spatial averaging (e.g. W_b of Jiang, 1994) and temporal averaging (e.g. mean W_n of Passchier, 1988; W_m of Bailey and Eyster, 2003; Bailey et al., 2004). Because of the explicitly instantaneous nature of W_b, we will use W_m throughout this manuscript, keeping in mind that we are interested in the bulk vorticity of a region (all components of a high-strain zone) over a period of time.

If flow in the deformation increment of interest has been steady-state, the instantaneous vorticity number W_k is equivalent to the mean vorticity number W_m. Tikoff and Fossen (1993, 1999) provide the following equation for the calculation of the kinematic vorticity number from a finite deformation matrix:

$$W_m \approx W_k = \frac{\sqrt{(\gamma_{yz})^2 + (\gamma_{xz})^2 + (\gamma_{xy})^2}}{\sqrt{2\left[\ln(k_1)^2 + \ln(k_2)^2 + \ln(k_3)^2\right] + (\gamma_{yz})^2 + (\gamma_{xz})^2 + (\gamma_{xy})^2}}. \tag{4}$$

This equation assumes steady-state deformation during the strain interval being quantified and therefore can be used to calculate W_k for a truly steady-state deformation or to

calculate W_m for a non-steady-state deformation. Note that this equation also assumes that the finite strain tensor has been rotated into a coordinate system defined relative to principal tectonic directions such that the matrix is upper-triangular (e.g. Flinn, 1979). An equation useful for calculating the kinematic vorticity number in more general flow regimes not described by upper-triangular matrices (e.g. triclinic flow) can be obtained by substituting Tikoff and Fossen's (1995) Eq. (8) into their Eq. (A9):

$$W_m \approx W_k = \frac{\sqrt{(\gamma_{zy}-\gamma_{yz})^2+(\gamma_{xz}-\gamma_{zx})^2+(\gamma_{yx}-\gamma_{xy})^2}}{\sqrt{2\left[\ln(k_1)^2+\ln(k_2)^2+\ln(k_3)^2\right]+(\gamma_{xy}+\gamma_{yx})^2+(\gamma_{xz}+\gamma_{zx})^2+(\gamma_{yz}+\gamma_{zy})^2}}. \quad (5)$$

Determination of the kinematic vorticity number alone is insufficient to uniquely characterize a non-plane-strain, three-dimensional deformation (Tikoff and Fossen, 1999). In order to distinguish between, for example, pure flattening and pure constriction deformations (both with $W_k = 0$), some qualitative description of fabric geometry must be considered in addition to the aspect ratio and orientation of the finite strain ellipsoid with respect to the shear plane.

2.6. Evaluation and interpretation of deformation path

After a high-strain zone has been thoroughly characterized and analyzed, the implications of the incremental deformation vorticities can be considered. The distinction between geometric steady-state and non-steady-state deformation paths is of particular interest. *A deformation path composed of strain increments having different vorticities defines a non-steady-state path*. Note that, although localizing and delocalizing zones can be analyzed in this manner, the steadiness of deformation in constant-volume high-strain zones (neither localizing nor delocalizing) cannot be evaluated from this analysis. Rather, the calculated vorticity values in a constant-volume zone describe the mean vorticity in each sub-zone over the entire length of finite deformation.

As described above, the complications inherent in interpreting three-dimensional kinematic vorticity (Tikoff and Fossen, 1999) are such that simple comparison of kinematic vorticity numbers between increments (for localizing or delocalizing zones) or sub-zones (for constant-volume zones) is insufficient to conclusively state whether or not those increments were produced along the same deformation path; strain and fabric data must also be considered in order to distinguish between possible kinematic boundary conditions described by the same kinematic vorticity number (e.g. pure flattening and pure constriction).

Results of this analysis can be interpreted as possible constraints on the deformation path followed by a high-strain zone. For example, evidence in a given high-strain zone of an early low vorticity phase of deformation preceding later high vorticity deformation limits the most likely deformation path appreciably. The true deformation path cannot be conclusively demonstrated, but any additional information is useful in analyses of deformed rocks, in which evidence is scant (Fossen and Tikoff, 1997).

3. Theoretical example

In order to demonstrate the procedure, we analyze a theoretical high-strain zone. As shown in Fig. 4, the zone has sub-vertical boundaries. For the purpose of demonstration, we assume that the spatial and temporal evolution of straining within the zone is unclear. Consequently, we will analyze the zone assuming both localizing and delocalizing end-member deformation histories. In Section 3.3 we discuss the constraints it is possible to place on the zone's deformation path based on consideration of both these histories.

We divide the high-strain zone into three sub-zones with increasing observed strain, $\mathbf{F}_1$, $\mathbf{F}_2$, and $\mathbf{F}_3$. Strain within each sub-zone is quantified and described within the coordinate system shown in Fig. 4. Now that the high-strain zone has been characterized, we calculate incremental strain based on the localizing and delocalizing deformation histories.

3.1. Localizing analysis

We first analyze the high-strain zone assuming deformation localized over time. The observed finite strain in the outermost sub-zone is $\mathbf{F}_1$. Because this sub-zone experienced only a single increment of deformation, the incremental deformation matrix describing deformation in that sub-zone is simply the finite strain observed in the sub-zone:

$$\mathbf{Z}_{L_1} = \mathbf{F}_1 = \begin{bmatrix} 1 & 0.5 & 0 \\ 0 & 1 & 0 \\ 0 & 0 & 1 \end{bmatrix}. \quad (6)$$

The finite strain recorded by the second sub-zone is $\mathbf{F}_2$. This finite strain accumulated by the superposition of two increments of deformation:

$$\mathbf{F}_2 = \mathbf{Z}_{L_2} \cdot \mathbf{Z}_{L_1} = \begin{bmatrix} 1 & 0.8 & 0 \\ 0 & 1 & 0 \\ 0 & 0 & 1 \end{bmatrix}. \quad (7)$$

The incremental finite strain in this sub-zone can be calculated by removing the effects of deformation in the outermost sub-zone:

$$\mathbf{Z}_{L_2} = \mathbf{F}_2 \cdot \mathbf{Z}_{L_1}^{-1} = \begin{bmatrix} 1 & 0.3 & 0 \\ 0 & 1 & 0 \\ 0 & 0 & 1 \end{bmatrix}. \quad (8)$$

where $\mathbf{Z}_{L_1}^{-1}$ is the matrix inverse of $\mathbf{Z}_{L_1}$.

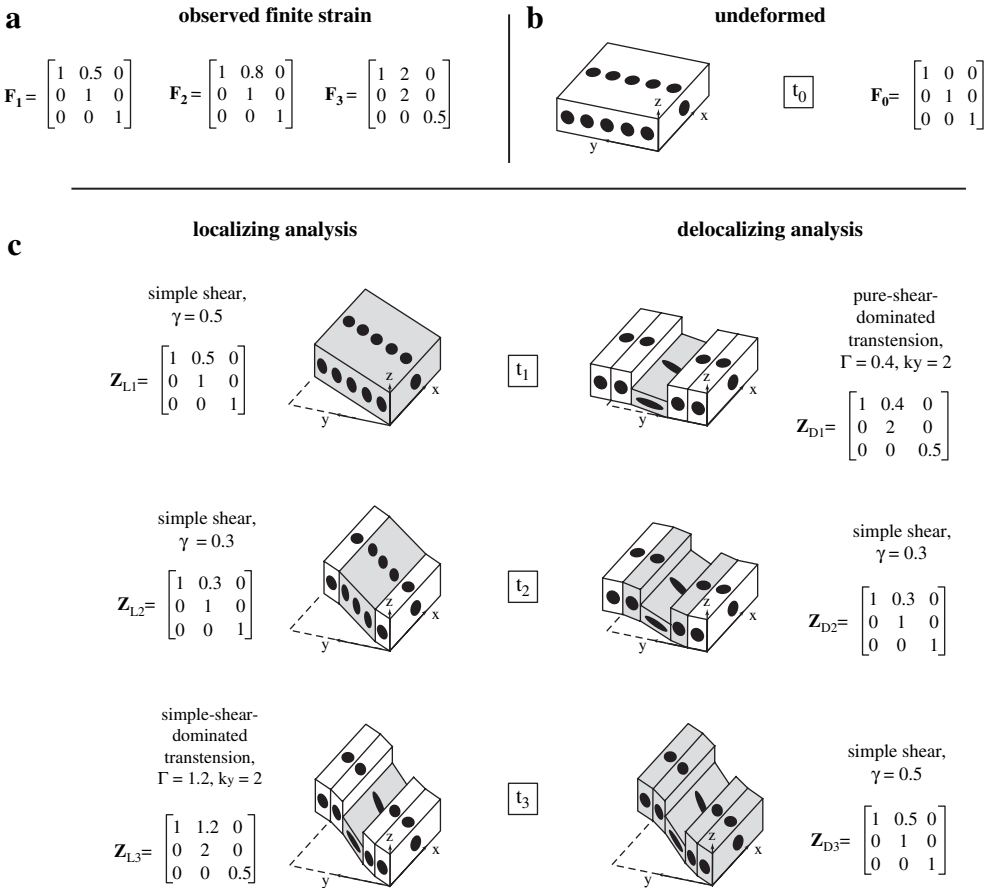

Fig. 4. Depiction and description of straining evolution in the theoretical high-strain zone as determined from localizing and delocalizing analyses. (a) Observed finite strain tensors $\mathbf{F}_i$ for the zone's three sub-zones. Bulk strain increases from $i = 1$ in the outer sub-zone to $i = 3$ in the innermost sub-zone. (b) Block diagram showing the assumed initial condition of the high-strain zone at time t_0, including the finite strain tensor $\mathbf{F}_0$. (c) Block diagrams showing the evolution of straining in the high-strain zone assuming progressive localization and delocalization. Shaded sub-zones in each of the time slices shown (t_1, t_2, t_3) indicate regions of active deformation. Strain ellipses are shown on all faces to indicate the three-dimensional strain in each sub-zone. Position gradient tensors for incremental deformation ($\mathbf{Z}_{L_i}$ for localizing and $\mathbf{Z}_{D_i}$ for delocalizing) are shown for each time slice. Note that the incremental deformations are different for the localizing and delocalizing zones.

The finite strain recorded by the third sub-zone is $\mathbf{F}_3$. This finite strain accumulated by the superposition of three increments of deformation:

$$\mathbf{F}_3 = \mathbf{Z}_{L_3} \cdot \mathbf{Z}_{L_2} \cdot \mathbf{Z}_{L_1} = \begin{bmatrix} 1 & 2 & 0 \\ 0 & 2 & 0 \\ 0 & 0 & 0.5 \end{bmatrix}. \tag{9}$$

Both $\mathbf{Z}_{L_2}$ and $\mathbf{Z}_{L_1}$ are known from analysis of the earlier two sub-zones, so the third increment of finite strain can be calculated:

$$\mathbf{Z}_{L_3} = \mathbf{F}_3 \cdot \mathbf{Z}_{L_1}^{-1} \cdot \mathbf{Z}_{L_2}^{-1} = \begin{bmatrix} 1 & 1.2 & 0 \\ 0 & 2 & 0 \\ 0 & 0 & 0.5 \end{bmatrix}. \tag{10}$$

Now that the increments of finite strain have been calculated for each sub-zone, the vorticity of these increments can be used to place constraints on deformation path.

Determining a vorticity value for each increment of deformation requires assumptions (e.g. monoclinic deformation) described in the vorticity analysis section above. The mean vorticity number within each sub-zone can be calculated from its deformation matrix (position gradient tensor) using Eq. (4). The mean vorticity numbers for the three increments of deformation $\mathbf{Z}_{L_1}$, $\mathbf{Z}_{L_2}$, and $\mathbf{Z}_{L_3}$ are $W_m = 1$, 1, and 0.51, respectively. These results are shown in Fig. 5.

Fig. 5a is a Nadai/Hsu diagram (e.g. Nadai, 1963; Hsu, 1966; Hossack, 1968; Owens, 1974; Brandon, 1995) that plots strain ellipsoid distortion (ε_s) against shape (ν). This diagram is similar to the familiar Flinn plot (Flinn, 1956, 1961) but is more informative in cases when it is desirable to separate the evolution of ellipsoid distortion and shape. The finite strain parameter ε_s is related to the octahedral unit shear of Nadai (1963), which is a measure of the amount or work required to distort a sphere ($\varepsilon_s = 0$) to a final shape ($\varepsilon_s > 0$). ε_s is defined as:

$$\varepsilon_s = \frac{1}{\sqrt{3}}\left[(\varepsilon_1 - \varepsilon_2)^2 + (\varepsilon_2 - \varepsilon_3)^2 + (\varepsilon_3 - \varepsilon_1)^2\right]^{\frac{1}{2}}, \tag{11}$$

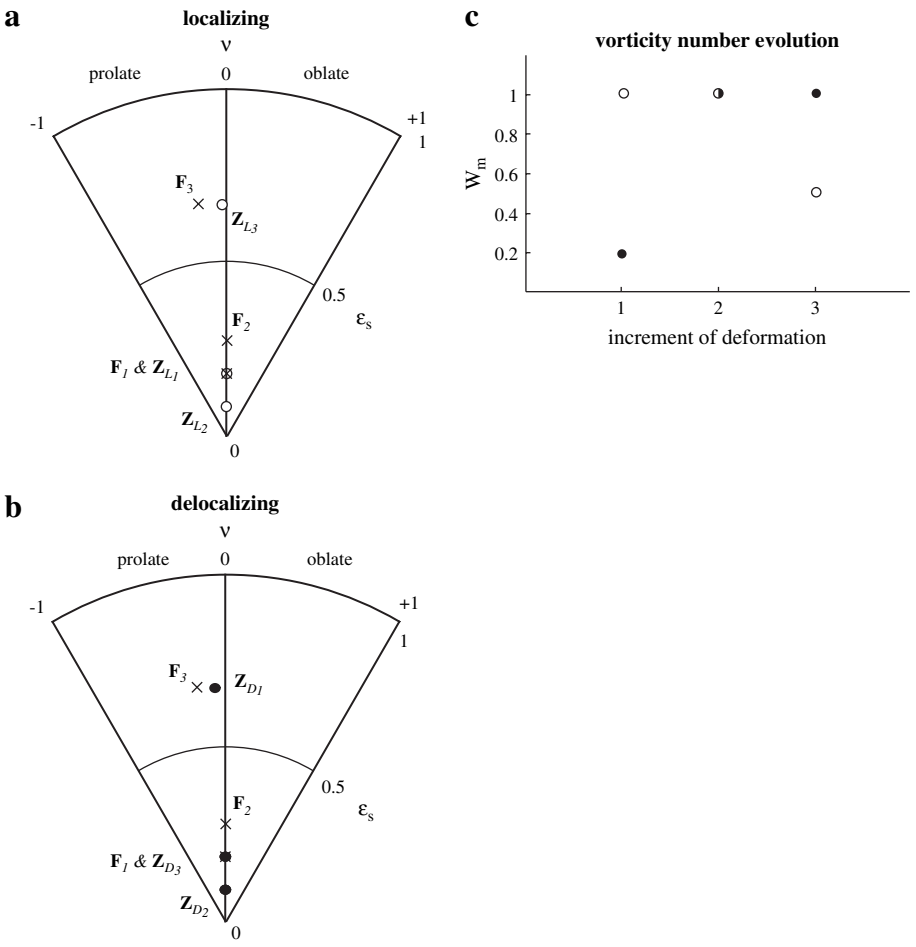

Fig. 5. (a) Nadai/Hsu diagram of strain ellipsoid distortion (ε_s) versus shape(ν) for sub-zones within the theoretical high-strain zone shown in Fig. 4. Symbols are plotted for observed finite strain ellipsoids ($\mathbf{F}_i$, crosses) and calculated incremental strain ellipsoids assuming localizing ($\mathbf{Z}_{L_i}$, open circles) deformation. (b) Nadai/Hsu diagram for observed finite strain ellipsoids ($\mathbf{F}_i$, crosses) and calculated incremental strain ellipsoids assuming delocalizing ($\mathbf{Z}_{D_i}$, filled circles) deformation. (c) Plot of mean kinematic vorticity number for each increment of deformation (1 is first, 3 is last) assuming the zone localized over time (open circles) or delocalized over time (filled circles). Changing values indicate non-steady-state deformation.

where ε_i are the natural logarithms of the principal stretches S_i of the strain ellipsoid. The ellipsoid shape is described by Lode's number ν, where:

$$\nu = \frac{2\varepsilon_2 - \varepsilon_1 - \varepsilon_3}{\varepsilon_1 - \varepsilon_3}. \tag{12}$$

Values of ν range from -1 (perfectly prolate) through 0 (plane strain) to $+1$ (perfectly oblate).

3.2. Delocalizing analysis

Assuming the high-strain zone delocalized over time, analysis follows the pattern outlined in Eq. (3) above. In this case, the final increment of deformation is recorded by the least deformed (outermost) sub-zone:

$$\mathbf{Z}_{D_3} = \mathbf{F}_1 = \begin{bmatrix} 1 & 0.5 & 0 \\ 0 & 1 & 0 \\ 0 & 0 & 1 \end{bmatrix}. \tag{13}$$

$\mathbf{Z}_{D_2}$ is calculated by removing the final increment of strain from the middle sub-zone:

$$\mathbf{Z}_{D_2} = \mathbf{Z}_{D_3}^{-1} \cdot \mathbf{F}_2 = \begin{bmatrix} 1 & 0.3 & 0 \\ 0 & 1 & 0 \\ 0 & 0 & 1 \end{bmatrix}. \tag{14}$$

The first increment of deformation is calculated by removing all of the temporally subsequent increments of strain from the highest-strain sub-zone:

$$\mathbf{Z}_{D_1} = \mathbf{Z}_{D_3}^{-1} \cdot \mathbf{Z}_{D_2}^{-1} \cdot \mathbf{F}_3 = \begin{bmatrix} 1 & 0.4 & 0 \\ 0 & 2 & 0 \\ 0 & 0 & 0.5 \end{bmatrix}. \tag{15}$$

In this delocalizing zone analysis, the first increment of deformation must have involved sinistral oblique divergence. The mean vorticities of each of the incremental strain matrices $\mathbf{Z}_{D_1}$, $\mathbf{Z}_{D_2}$, and $\mathbf{Z}_{D_3}$ are $W_m = 0.2$, 1, and 1, respectively. These results are shown in Fig. 5.

3.3. Deformation path interpretation

The vorticity results for the localizing and delocalizing analyses (Fig. 5) suggest that the deformation path for the zone was non-steady-state. In Fig. 5a the incremental

ellipsoids $\mathbf{Z}_{L_1}$ and $\mathbf{Z}_{L_2}$ for localizing analysis plot on the plane strain line ($\nu = 0$), as expected for simple shear kinematics. Similarly, the incremental ellipsoids $\mathbf{Z}_{D_2}$ and $\mathbf{Z}_{D_3}$ for delocalizing deformation plot on the plane strain line. However, the results indicate that one increment of deformation is clearly non-plane strain ($\mathbf{Z}_{L_3}$ or $\mathbf{Z}_{D_1}$). These same observations are clear when looking at the specific mean vorticity values (Fig. 5c). In both cases, two increments of deformation involved simple shear kinematics while the third increment involved a significant pure shear component in addition to a simple shear component. The temporal order of the different kinematic boundary conditions, however, varies depending on whether the zone localized or delocalized.

Simple observation of the incremental vorticity numbers is insufficient to fully interpret the deformation path because of the ambiguity inherent in three-dimensional vorticity analysis (Tikoff and Fossen, 1999). Strain facies observations (Hansen, 1971) provide important information about deformation geometry (Tikoff and Fossen, 1999). In this case, the prolate shape of the ellipsoid (Fig. 4) in the innermost sub-zone indicates constriction rather than flattening. This suggests that bulk transtension rather than transpression produced the observed strain.

4. Natural example 1: kilometer-scale analysis

Zhang and Hynes (1995) present three-dimensional finite strain data from a km-scale high-strain zone in north-central British Columbia. Their data describe strain within a deformed Late Triassic volcanic breccia. They assume clasts within the breccia behaved passively during a constant-volume monoclinic deformation. They used a coordinate system in which the z-axis is perpendicular to the high-strain zone boundary (unexposed but assumed planar and parallel to the well developed cleavage), the x-axis is horizontal within the shear plane, and the y-axis points up-dip on the shear plane. Zhang and Hynes (1995) divided the high-strain zone into three sub-zones, each of which exhibits roughly homogeneous finite strain shape and magnitude. They calculated a position gradient tensor for each of these sub-zones. To accomplish this they assumed that finite strain in each of the sub-zones accumulated due to simultaneous coaxial stretching parallel to three coordinate axes and simple shearing parallel to the x-axis. Their calculated position gradient tensors, in order from relatively low-strain magnitude ($\mathbf{F}_1$) to high magnitude ($\mathbf{F}_3$), are as follows. Note that the calculations to four decimal places are from Zhang and Hynes (1995).

$$\mathbf{F}_1 = \begin{bmatrix} 1.5891 & 0.8758 & 0 \\ 0 & 0.5422 & 0 \\ 0 & 0 & 1.1807 \end{bmatrix}, \tag{16}$$

$$\mathbf{F}_2 = \begin{bmatrix} 1.3460 & 1.3518 & 0 \\ 0 & 0.5940 & 0 \\ 0 & 0 & 1.2510 \end{bmatrix}, \text{ and} \tag{17}$$

$$\mathbf{F}_3 = \begin{bmatrix} 0.6616 & 8.1025 & 0 \\ 0 & 2.7687 & 0 \\ 0 & 0 & 0.5511 \end{bmatrix}. \tag{18}$$

Zhang and Hynes (1995) attempted to reproduce their strain data using a steady-state forward model. They were unsuccessful because no monoclinic, constant-volume, steady-state deformation path can move from the field of apparent flattening ($\mathbf{F}_1$ and $\mathbf{F}_2$) to the field of apparent constriction ($\mathbf{F}_3$). Within the constraints of their assumptions (in particular, monoclinic deformation), Zhang and Hynes' data indicate a non-steady-state deformation path. The analysis presented here allows us to place additional constraints on the nature of the non-steady-state deformation.

Based on fabric transposition evidence, Zhang and Hynes (1995) suggest that deformation progressively localized in the high-strain zone they characterized. Despite this assumption, we analyze their data from both localizing and delocalizing zone perspectives. This generalized approach allows us to confidently draw conclusions about the nature of the kinematic evolution recorded by finite strain in the zone.

4.1. Localizing zone analysis

Calculation of incremental deformation tensors follows the procedure outlined in Eq. (2) above for localizing high-strain zones. If the rock was initially undeformed the incremental position gradient tensors are:

$$\mathbf{Z}_{L_1} = \mathbf{F}_1 = \begin{bmatrix} 1.5891 & 0.8758 & 0 \\ 0 & 0.5422 & 0 \\ 0 & 0 & 1.1807 \end{bmatrix}, \tag{19}$$

$$\mathbf{Z}_{L_2} = \mathbf{F}_2 \cdot \mathbf{Z}_{L_1}^{-1} = \begin{bmatrix} 0.8470 & 1.1250 & 0 \\ 0 & 1.0955 & 0 \\ 0 & 0 & 1.0595 \end{bmatrix}, \text{ and} \tag{20}$$

$$\mathbf{Z}_{L_3} = \mathbf{F}_3 \cdot \mathbf{Z}_{L_1}^{-1} \cdot \mathbf{Z}_{L_2}^{-1} = \begin{bmatrix} 0.4915 & 12.5220 & 0 \\ 0 & 4.6611 & 0 \\ 0 & 0 & 0.4405 \end{bmatrix}. \tag{21}$$

By multiplying these incremental deformation tensors together in the proper sequence ($\mathbf{Z}_{L_1}$ first, $\mathbf{Z}_{L_2}$ second, and $\mathbf{Z}_{L_3}$ third), it is possible to check that they produce the observed $\mathbf{F}_3$ tensor:

$$\mathbf{Z}_{L_3} \cdot \mathbf{Z}_{L_2} \cdot \mathbf{Z}_{L_1} = \begin{bmatrix} 0.6616 & 8.1025 & 0 \\ 0 & 2.7687 & 0 \\ 0 & 0 & 0.5511 \end{bmatrix}. \tag{22}$$

Again using Eq. (4), the mean vorticity numbers of the $\mathbf{Z}_{L_1}$, $\mathbf{Z}_{L_2}$, and $\mathbf{Z}_{L_3}$ incremental deformations are $W_m = 0.63$, 0.97, and 0.93, respectively. These results are shown in Fig. 6.

4.2. Delocalizing zone analysis

The same observed finite strains can be analyzed assuming they formed in an delocalizing high-strain zone. The mathematical procedures for isolating the finite strain increments

follow Eq. (3). In the case of a delocalizing high-strain zone, the incremental strain tensors corresponding to Zhang and Hynes' (1995) strain gradient are as follows:

$$\mathbf{Z}_{D_3} = \mathbf{F}_1 = \begin{bmatrix} 1.5891 & 0.8758 & 0 \\ 0 & 0.5422 & 0 \\ 0 & 0 & 1.1807 \end{bmatrix}, \quad (23)$$

$$\mathbf{Z}_{D_2} = \mathbf{Z}_{D_3}^{-1} \cdot \mathbf{F}_2 = \begin{bmatrix} 0.8470 & 0.2469 & 0 \\ 0 & 1.0955 & 0 \\ 0 & 0 & 1.0595 \end{bmatrix}, \text{ and} \quad (24)$$

$$\mathbf{Z}_{D_1} = \mathbf{Z}_{D_2}^{-1} \cdot \mathbf{Z}_{D_3}^{-1} \cdot \mathbf{F}_3 = \begin{bmatrix} 0.4915 & 1.3385 & 0 \\ 0 & 4.6611 & 0 \\ 0 & 0 & 0.4405 \end{bmatrix}. \quad (25)$$

As with the localizing zone analysis, multiplying these tensors together in the proper sequence ($\mathbf{Z}_{D_1}$ first, $\mathbf{Z}_{D_2}$ second, and $\mathbf{Z}_{D_3}$ third) produces the observed $\mathbf{F}_3$ tensor:

$$\mathbf{Z}_{D_3} \cdot \mathbf{Z}_{D_2} \cdot \mathbf{Z}_{D_1} = \begin{bmatrix} 0.6616 & 8.1025 & 0 \\ 0 & 2.7687 & 0 \\ 0 & 0 & 0.5511 \end{bmatrix}. \quad (26)$$

However, in this case the mean vorticity numbers of each of the incremental strain matrices $\mathbf{Z}_{D_1}$, $\mathbf{Z}_{D_2}$, and $\mathbf{Z}_{D_3}$ are $W_m = 0.26$, 0.67, and 0.63, respectively. These results are shown in Fig. 6.

4.3. Deformation path evaluation

Both the localizing and delocalizing analyses demonstrate that the observed deformation must be the result of non-steady-state kinematics. Both analyses (Fig. 6) suggest the first increment of finite strain ($\mathbf{Z}_1$) had a significantly lower mean vorticity than the second two increments ($\mathbf{Z}_2$ and $\mathbf{Z}_3$), which requires non-steady-state deformation. The analyses' parallel recognition of an early, relatively low vorticity phase of deformation suggests that this is a robust result; the deformation path likely evolved from an early relatively low vorticity phase

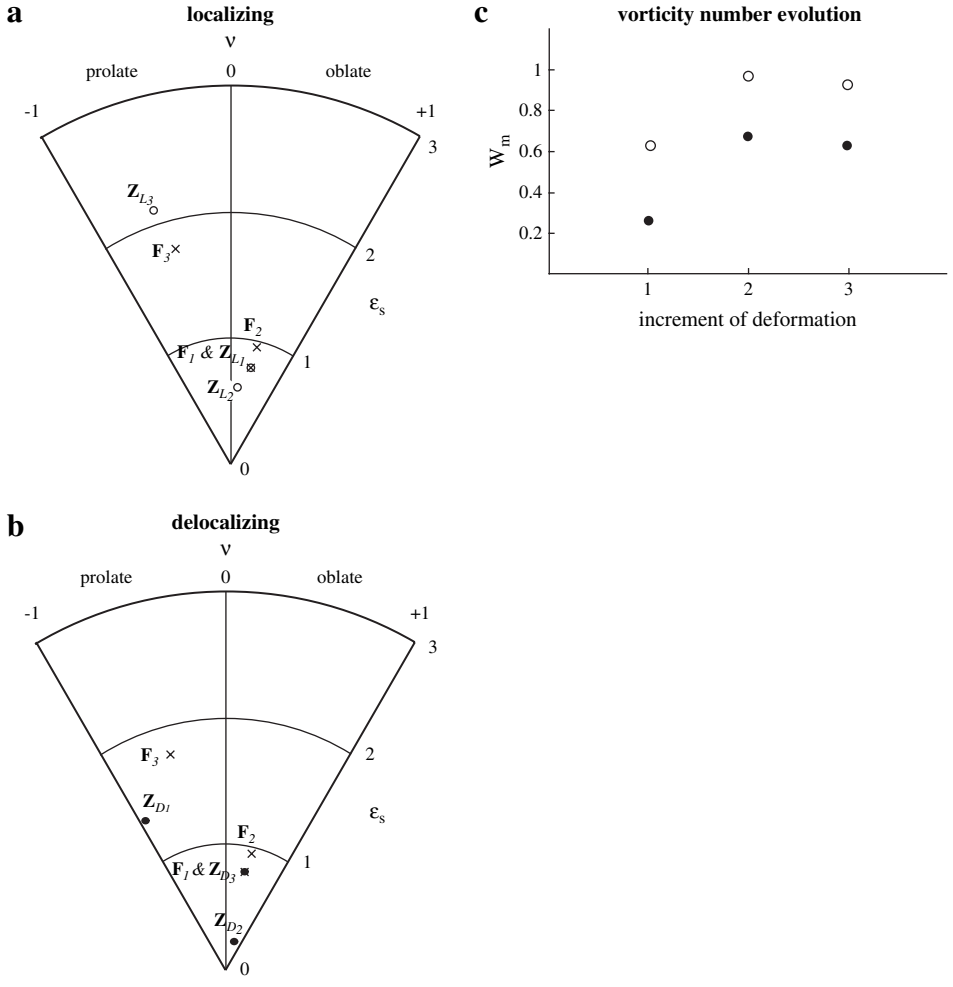

Fig. 6. (a) Nadai/Hsu diagram of strain ellipsoid distortion (ε_s) versus shape (ν) for sub-zones within the high-strain zone described by Zhang and Hynes (1995). Symbols are plotted for observed finite strain ellipsoids ($\mathbf{F}_i$, crosses) and calculated incremental strain ellipsoids assuming localizing ($\mathbf{Z}_{L_i}$, open circles) deformation. (b) Nadai/Hsu diagram for observed finite strain ellipsoids ($\mathbf{F}_i$, crosses) and calculated incremental strain ellipsoids assuming delocalizing ($\mathbf{Z}_{D_i}$, filled circles) deformation. (c) Plot of mean kinematic vorticity number for each increment of deformation (1 is first, 3 is last) assuming the zone localized over time (open circles) or delocalized over time (filled circles). Changing values indicate non-steady-state deformation.

into a subsequent phase with a significantly higher vorticity. The change from broadly flattening strain in the outer sub-zones ($\mathbf{F}_1$ and $\mathbf{F}_2$) to strongly constructional strain in the more deformed sub-zone ($\mathbf{F}_3$) is further evidence of a change in kinematic boundary conditions.

5. Natural example 2: centimeter-scale analysis

Bhattacharyya and Hudleston (2001) conducted three-dimensional strain analysis on cm-scale meta-gabbro high-strain zones in the Seve Nappe Complex of the Upper Allochthon of the northern Scandinavian Caledonides. The high-strain zones analyzed are part of a complicated anastomosing three-dimensional network that accommodated regional deformation. Because the high-strain zones that Bhattacharyya and Hudleston (2001) analyzed are only a small part of a larger network, extrapolating results to larger scales is not possible. However, analyses like these provide important information about high-strain zone kinematics in cases where the system is relatively well understood.

The analysis presented here is concerned with Sample 1 from Bhattacharyya and Hudleston (2001), in which the 10-cm-thick high-strain zone is defined by deformation of plagioclase aggregates (see their Fig. 8). Because the relationship between local and regional deformation was beyond the scope of their paper, Bhattacharyya and Hudleston (2001) defined a coordinate system in which the presumed shearing direction was oriented 01 → 355 and the shear plane was oriented 182/06W. By analyzing sub-zones of approximately homogeneous strain Bhattacharyya and Hudleston (2001) calculated 13 strain ellipsoids across the high-strain zone by combining two-dimensional plagioclase strain data (using the method of Wheeler, 1986) collected using R_f/ϕ analysis (e.g. Ramsay, 1967, pp. 202–211; Lisle, 1977, 1979, 1985; Lisle et al., 1983). We consider the results from ellipsoids 1 to 10 because they comprise a complete profile across one side of the zone; ellipsoids 11–13 are located on the other side of the high-strain zone and are not considered further here.

5.1. Localizing and delocalizing zone analyses

Bhattacharyya and Hudleston (2001) assumed that deformation within the high-strain zone localized progressively over time. Despite this assumption, unequivocal evidence of the zone's geometric evolution is lacking. We therefore analyzed the calculated position gradient tensors using both localizing and delocalizing zone mathematical frameworks. Consequently, our analysis follows the frameworks outlined in Eqs. (2) and (3) above, for localizing and delocalizing zones, respectively.

We calculated finite stretch tensors (Ramsay, 1967, p. 124; Elliott, 1972; Flinn, 1978; Means, 1994; Zhang and Hynes, 1995) for zones 1–10 from the eigenvalues and eigenvectors of each sub-zone's observed strain ellipsoid (provided by P. Bhattacharyya, personal communication, 2005). Each of these stretch tensors was rotated into the coordinate system defined by the shear zone axes to produce an individual position gradient tensor for each sub-zone (Appendix B). Ten incremental position gradient tensors were then calculated from the observed position gradient tensors for both localizing and delocalizing zones (Appendix B). The mean vorticity number of each incremental tensor was then calculated using Eq. (4) above (Table 1 and Fig. 7).

5.2. Deformation path evaluation

As is clear from the vorticity results shown on Fig. 7, the finite strain within the high-strain zone cannot be explained with a steady-state deformation path. Note, however, that the localizing zone analysis suggests that the early history of the deformation was roughly steady-state. For the localizing analysis, the mean vorticity number in increments 1–7 is approximately $W_m = 0.9$ (+/− 0.05) but falls to generally lower values in increments 8–10. In contrast, for the delocalizing analysis the mean vorticity number generally increases throughout deformation. These results suggest that, if Bhattacharyya and Hudleston's (2001) assumption of a localizing zone is accurate, this high-strain zone likely had an early high vorticity deformation history before recording a period of lower vorticity. However, if their assumption is incorrect it is difficult to confidently conclude anything about the deformation path aside from its non-steady-state nature. Regardless, the flattening nature of the strain throughout the high-strain zone is consistent with a general transpressional deformation path.

6. Discussion

The non-unique nature of deformation path has been discussed by many authors (e.g. Elliott, 1972; Passchier, 1988; Jiang, 1994; Fossen and Tikoff, 1997), but most of the infinite possible paths for a given observed deformation are unrealistic (Provost et al., 2004). Recognition of even a few points along a high-strain zone's likely deformation path dramatically limits the range of possible paths. The analyses we present here demonstrate that even in instances where it is difficult or impossible to determine the spatial and temporal evolution

Table 1
Mean vorticity numbers for Bhattacharyya and Hudleston's (2001) strain data

Observed tensor	W_m	Incremental tensor	W_m, localizing	W_m, delocalizing
$\mathbf{F}_1$	0.90	$\mathbf{Z}_1$	0.90	0.04
$\mathbf{F}_2$	0.90	$\mathbf{Z}_2$	0.88	0.27
$\mathbf{F}_3$	0.90	$\mathbf{Z}_3$	0.79	0.96
$\mathbf{F}_4$	0.87	$\mathbf{Z}_4$	0.91	0.34
$\mathbf{F}_5$	0.91	$\mathbf{Z}_5$	0.83	0.80
$\mathbf{F}_6$	0.88	$\mathbf{Z}_6$	0.92	0.51
$\mathbf{F}_7$	0.50	$\mathbf{Z}_7$	0.37	0.75
$\mathbf{F}_8$	0.39	$\mathbf{Z}_8$	1.00	0.80
$\mathbf{F}_9$	0.40	$\mathbf{Z}_9$	0.41	0.86
$\mathbf{F}_{10}$	0.42	$\mathbf{Z}_{10}$	0.60	0.90

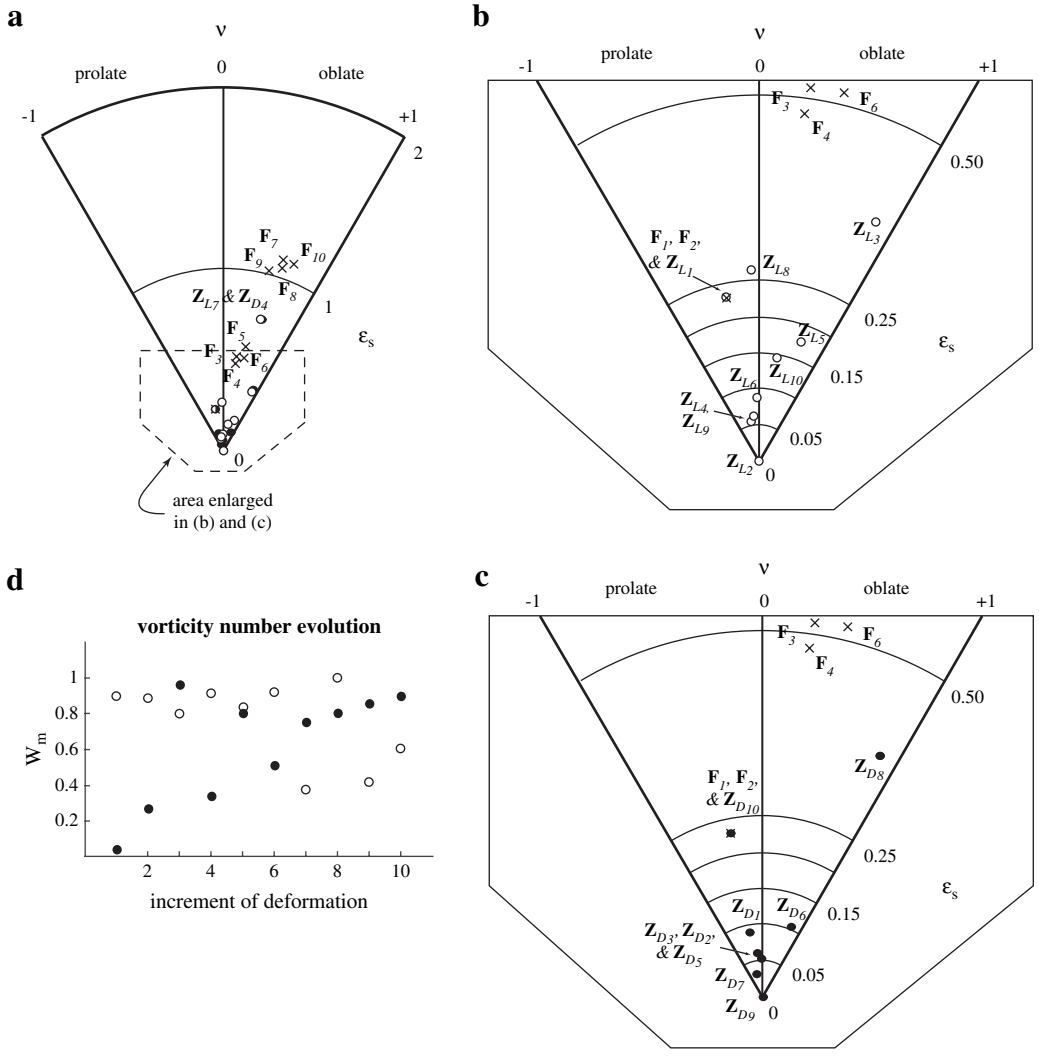

Fig. 7. (a) Nadai/Hsu diagram of strain ellipsoid distortion (ε_s) versus shape (ν) for sub-zones within the high-strain zone described by Bhattacharyya and Hudleston (2001). Symbols are plotted for observed finite strain ellipsoids ($\mathbf{F}_i$, crosses) and calculated incremental strain ellipsoids assuming localizing ($\mathbf{Z}_{L_i}$, open circles) delocalizing ($\mathbf{Z}_{D_i}$, filled circles) and constant-volume (crosses) deformation. Dashed box shows area enlarged in (b) and (c). (b) Enlargement of the area shown in (a) plotting only the data for observed finite strain ellipsoids and calculated localizing zone incremental strain. (c) Enlargement of the area shown in (a) plotting only the data for observed finite strain ellipsoids and calculated delocalizing zone incremental strain. (d) Plot of mean kinematic vorticity number for each increment of deformation (1 is first, 10 is last) assuming the zone localized over time (open circles) or delocalized over time (filled circles). Changing values indicate non-steady-state deformation.

of straining in a high-strain zone, it is sometimes possible to extract broad patterns of kinematic evolution from finite strain gradients. This information is important because it dramatically reduces the possible range of deformation paths followed by the zone.

For example, in the case of the zone described by Zhang and Hynes (1995), two main points pertinent to deformation path analysis can be extracted from the finite strain data. First, the zone followed a non-steady-state deformation path. Second, that deformation path likely includes an early low vorticity period of deformation followed by a later higher vorticity period. Clearly, this information does not uniquely identify the zone's deformation path, but it does narrow considerably the possible tectonic interpretations of the finite strain data.

As the Zhang and Hynes example demonstrates, an additional product of this methodology is that it allows us to test the common assumption of kinematic steady-state deformation behavior. In both natural examples we analyzed, deformation was clearly non-steady-state. Most natural shear zones probably form as a result of non-steady-state deformation (e.g. Passchier, 1988; Jiang and White, 1995; Tikoff and Fossen, 1995; Montesi and Hirth, 2003) but few methodologies to test this assertion have been presented.

Applicability of this methodology is limited by both the simplified mathematical framework as presented here and by the complexity and uncertainty inherent in analysis of naturally deformed rocks. For simplicity's sake, the methodology is described using monoclinic kinematic models. However, high-strain zones with triclinic symmetry can be analyzed in

a similar manner provided the direction of simple shearing relative to the directions of pure shearing in each sub-zone can be constrained. Information about the relative orientations of simple and pure shearing can be collected or inferred in some high-strain zones (e.g. Lin et al., 1998) and the common assumption of monoclinic deformation can be tested with observations of the high-strain zone. For example, if the maximum asymmetry of shear sense indicators is observed on a plane roughly perpendicular to both foliation and the direction of simple shearing, deformation can be reasonably assumed monoclinic (Jiang and White, 1995). Similarly, the presence of stretching lineations that are neither parallel nor perpendicular to the direction of simple shearing suggests triclinic deformation symmetry. Note however that triclinic deformation proceeding to R_s greater than $\sim$10 produces lineations with apparent monoclinic symmetry (Jiang and Williams, 1998; Lin et al., 1998).

Purely kinematic analyses such at that presented here must be applied with caution because the mechanical feasibility of results has not been rigorously addressed. It may be possible to calculate deformation paths that are unlikely or impossible for the mechanical properties of the rocks under consideration. Mechanical heterogeneity is generally thought to strongly influence relative deformation behavior (e.g. Cobbold et al., 1971; Cobbold, 1976; Treagus et al., 1983; Treagus, 1988, 1993; Ishii, 1992; Weijermars, 1992; Simpson and DePaor, 1993; Jiang and White, 1995; Goodwin and Tikoff, 2002), but field observations do not always bear this out (e.g. Piazolo and Passchier, 2002). In general, purely kinematic methodologies may be best suited to analysis of homogeneous or nearly homogeneous bodies of rock. Because the distinction between homogeneous and heterogeneous is often scale dependent (Turner and Weiss, 1963, pp. 16–17), the inherent scale independence of finite strain makes it an attractive and useful tool on which to base an analysis methodology. However, we believe this method has the potential to shed light on feedback relationships between straining and the mechanical evolution of rocks. It is possible that rheological thresholds in the evolution of high-strain zones may be recognized from this purely kinematic analysis. Further evaluation of such thresholds must rely upon additional mechanical analysis.

An important source of error in our analysis results stems from uncertainty in strain calculations (e.g. Dunnet and Siddans, 1971; Cutler, 1985; Schultz-Ela, 1990; Yamaji, 2005). For the Zhang and Hynes example, we calculate that 25% error in the magnitude of the finite strain ellipsoid axes results in roughly 5% change in the calculated mean vorticity number. This calculation is highly situation dependent, but provides a rough idea of the magnitude of the effects that strain measurement error can produce.

Another limitation of the methodology and many geological analyses of natural deformation is related to the difficulty with defining boundaries between domains with gradational contacts. Both Zhang and Hynes (1995) and Bhattacharyya and Hudleston (2001) acknowledge that the boundaries between the sub-zones they defined are somewhat arbitrary in that observed differences in fabric orientation or appearance were used to estimate boundaries. These difficulties result in apparent strain compatibility problems between sub-zones and between the high-strain zone and wallrock. Additionally, variations in sub-zone definition can produce different analysis results. Many of these issues can, in theory, be resolved or minimized by analyzing deformed systems at different spatial scales.

The results we present also lead to the question of how steady-state deformation should be defined when dealing with the uncertainty inherent in consideration of rocks. For instance, it is difficult to rigorously define a cut-off value in two increments' mean vorticity values above which those sub-zones record non-steady-state kinematics. We consider the changes in calculated mean vorticity numbers for both Zhang and Hynes' (1995) analysis (between increments 1 and 2, regardless of localizing or delocalizing) and Bhattacharyya and Hudleston's (2001) analysis (between sub-zones 1–6 and 7–10) to suggest non-steady-state deformation. This issue may be best considered on a case-by-case basis until we have a firmer grasp of the range and significance of observed deformation paths.

7. Conclusions

By understanding the spatial and temporal distribution of straining in high-strain zones, the kinematic history recorded in the rocks can be studied by mathematically removing strain fields. The general analysis procedure is as follows. (1) The geometric evolution of the high-strain zone is characterized. (2) The zone is subdivided into component sub-zones, each of which has roughly homogeneous finite strain magnitude, shape, and orientation. (3) Finite strain is measured in each sub-zone. (4) Incremental strains are calculated from the observed finite strain using equations for localizing or delocalizing zones. (5) The mean kinematic vorticity number of each strain increment is calculated. (6) Using a combination of observations (strain facies, fabric orientation) and calculated results (incremental deformation tensors), the zone's likely deformation path is considered.

Knowledge of the spatial and temporal evolution of straining within the high-strain zone is an essential prerequisite to constraining possible deformation paths. Although we discuss analysis procedures for three end-member geometric straining histories, more complicated histories can be analyzed provided that the straining history can be worked out. However, even in cases where the spatial and temporal evolution of strain is difficult or impossible to decipher, it is sometimes possible to determine some basic information about high-strain zone kinematics like the presence or absence of a steady-state kinematic history.

The analysis produces non-unique results. However, the purpose of strain gradient analysis is to place constraints on possible deformation paths rather than to identify the true path. Although an infinite number of possible deformation paths could theoretically have produced a given observed strain gradient, some paths are more likely than others and any constraints we can place are beneficial and useful.

Acknowledgements

This work was supported by in part by a Ciriacks graduate fellowship to EH. We thank Haakon Fossen for helpful discussions and Juk Bhattacharyya for providing both published and unpublished strain data from the Caledonides. Scott Giorgis, Stephanie Maes, and Sarah Titus read early drafts of this manuscript and their suggestions were extremely helpful. We are grateful to Matty Mookerjee for helpful clarifying comments and to Chuck Bailey and Marcia Bjornerud for thorough, thoughtful reviews.

Appendix A. Derivation of Eqs. (2) and (3)

The different ways in which straining evolves spatially in localizing and delocalizing high-strain zones require slightly different procedures for isolating increments of finite strain. Both procedures, however, involve successively removing increments of strain observed in relatively little-deformed sub-zones from strain observed in more deformed sub-zones. The different procedures sometimes result in different incremental tensors for localizing ($\mathbf{Z}_{L_i}$) and delocalizing sub-zones ($\mathbf{Z}_{D_i}$). Note also that similar procedures can be used to examine more complicated straining histories than those discussed in this manuscript.

For the localizing analysis, the procedure can be conceptualized by first recalling that the outermost sub-zone in a localizing high-strain zone ($\mathbf{F}_1$) records only the first increment of deformation ($\mathbf{Z}_{L_1}$), so $\mathbf{Z}_{L_1} = \mathbf{F}_1$. The adjacent sub-zone ($\mathbf{F}_2$) records both the first and second increments of deformation ($\mathbf{Z}_{L_1}$ and $\mathbf{Z}_{L_2}$);

$$\mathbf{F}_2 = \mathbf{Z}_{L_2} \cdot \mathbf{Z}_{L_1} \tag{A1}$$

The second increment of deformation is calculated by isolating $\mathbf{Z}_{L_2}$ in Eq. (A1). This goal can be accomplished by multiplying both sides of Eq. (A1) by $\mathbf{Z}_{L_1}^{-1}$, the matrix inverse of $\mathbf{Z}_{L_1}$:

$$\mathbf{F}_2 \cdot \mathbf{Z}_{L_1}^{-1} = \mathbf{Z}_{L_2} \cdot \mathbf{Z}_{L_1} \cdot \mathbf{Z}_{L_1}^{-1}, \tag{A2a}$$

which simplifies to:

$$\mathbf{F}_2 \cdot \mathbf{Z}_{L_1}^{-1} = \mathbf{Z}_{L_2}. \tag{A2b}$$

Sub-zone $\mathbf{F}_3$ records three increments of deformation:

$$\mathbf{F}_3 = \mathbf{Z}_{L_3} \cdot \mathbf{Z}_{L_2} \cdot \mathbf{Z}_{L_1}. \tag{A3}$$

The third increment of deformation is calculated by isolating $\mathbf{Z}_{L_3}$ in Eq. (A3). Again, this can be accomplished by sequentially removing increments of deformation already calculated. In this case, $\mathbf{Z}_{L_1}$ is removed before $\mathbf{Z}_{L_2}$:

$$\mathbf{F}_3 \cdot \mathbf{Z}_{L_1}^{-1} = \mathbf{Z}_{L_3} \cdot \mathbf{Z}_{L_2} \cdot \mathbf{Z}_{L_1} \cdot \mathbf{Z}_{L_1}^{-1}, \tag{A4a}$$

which simplifies to:

$$\mathbf{F}_3 \cdot \mathbf{Z}_{L_1}^{-1} = \mathbf{Z}_{L_3} \cdot \mathbf{Z}_{L_2}. \tag{A4b}$$

To isolate $\mathbf{Z}_{L_3}$ the procedure is followed once more using the inverse of $\mathbf{Z}_{L_2}$:

$$\mathbf{F}_3 \cdot \mathbf{Z}_{L_1}^{-1} \cdot \mathbf{Z}_{L_2}^{-1} = \mathbf{Z}_{L_3} \cdot \mathbf{Z}_{L_2} \cdot \mathbf{Z}_{L_2}^{-1}, \tag{A5a}$$

which simplifies to:

$$\mathbf{F}_3 \cdot \mathbf{Z}_{L_1}^{-1} \cdot \mathbf{Z}_{L_2}^{-1} = \mathbf{Z}_{L_3}. \tag{A5b}$$

The pattern can be followed to isolate increments of deformation in a localizing high-strain zone composed of any number of increments.

Deriving Eq. (3), which describes how to calculate increments of finite strain in a delocalizing high-strain zone, is again accomplished by progressively isolating strain increments of interest. However, the strain evolution pattern in a delocalizing zone differs from that in a localizing zone and therefore requires a slightly different isolation procedure. Recall that in a delocalizing high-strain zone that formed through the superposition of an arbitrary number of increments $\mathbf{Z}_{D_i}$ (for $1 \leq i \leq n$), the outermost sub-zone ($\mathbf{F}_1$) records only the final increment of deformation ($\mathbf{Z}_{D_n}$). Thus, $\mathbf{Z}_{D_n} = \mathbf{F}_1$. The adjacent sub-zone $\mathbf{F}_2$ records both the last and penultimate increments of deformation:

$$\mathbf{F}_2 = \mathbf{Z}_{D_n} \cdot \mathbf{Z}_{D_{n-1}}. \tag{A6}$$

$\mathbf{Z}_{D_{n-1}}$ is isolated by multiplying both sides of Eq. (A6) by $\mathbf{Z}_{D_n}^{-1}$. The non-commutative nature of matrix multiplication requires left multiplication in this case:

$$\mathbf{Z}_{D_n}^{-1} \cdot \mathbf{F}_2 = \mathbf{Z}_{D_n}^{-1} \cdot \mathbf{Z}_{D_n} \cdot \mathbf{Z}_{D_{n-1}}, \tag{A7a}$$

which simplifies to:

$$\mathbf{Z}_{D_n}^{-1} \cdot \mathbf{F}_2 = \mathbf{Z}_{D_{n-1}}. \tag{A7b}$$

Sub-zone $\mathbf{F}_3$ records the final three increments of deformation:

$$\mathbf{F}_3 = \mathbf{Z}_{D_n} \cdot \mathbf{Z}_{D_{n-1}} \cdot \mathbf{Z}_{D_{n-2}}. \tag{A8}$$

$\mathbf{Z}_{D_{n-2}}$ is isolated by sequentially multiplying both sides of Eq. (A6) by $\mathbf{Z}_{D_n}^{-1}$ and $\mathbf{Z}_{D_{n-1}}^{-1}$. In this case $\mathbf{Z}_{D_n}$ is removed before $\mathbf{Z}_{D_{n-1}}$:

$$\mathbf{Z}_{D_n}^{-1} \cdot \mathbf{F}_3 = \mathbf{Z}_{D_n}^{-1} \cdot \mathbf{Z}_{D_n} \cdot \mathbf{Z}_{D_{n-1}} \cdot \mathbf{Z}_{D_{n-2}}, \tag{A9a}$$

which simplifies to:

$$\mathbf{Z}_{D_n}^{-1} \cdot \mathbf{F}_3 = \mathbf{Z}_{D_{n-1}} \cdot \mathbf{Z}_{D_{n-2}}. \tag{A9b}$$

To isolate $\mathbf{Z}_{D_{n-2}}$, the procedure is followed once more using the inverse of $\mathbf{Z}_{D_{n-1}}$:

$$\mathbf{Z}_{D_{n-1}}^{-1} \cdot \mathbf{Z}_{D_n}^{-1} \cdot \mathbf{F}_3 = \mathbf{Z}_{D_{n-1}}^{-1} \cdot \mathbf{Z}_{D_{n-1}} \cdot \mathbf{Z}_{D_{n-2}}, \tag{A10a}$$

which simplifies to:

$$\mathbf{Z}_{D_{n-1}}^{-1} \cdot \mathbf{Z}_{D_n}^{-1} \cdot \mathbf{F}_3 = \mathbf{Z}_{D_{n-2}}. \tag{A10b}$$

The pattern can be followed to isolate increments of deformation in a delocalizing high-strain zone composed of any number of increments.

Appendix B. Finite and incremental position gradient tensors for Bhattacharyya and Hudleston (2001)

Observed finite strain	Calculated incremental strain - localizing	Calculated incremental strain - delocalizing
$\mathbf{F}_0 = \begin{bmatrix} 1 & 0 & 0 \\ 0 & 1 & 0 \\ 0 & 0 & 1 \end{bmatrix}$		
$\mathbf{F}_1 = \begin{bmatrix} 1.14 & 0 & 0.47 \\ 0 & 0.95 & 0 \\ 0 & 0 & 0.94 \end{bmatrix}$	$\mathbf{Z}_{L_1} = \begin{bmatrix} 1.14 & 0 & 0.47 \\ 0 & 1.00 & 0 \\ 0 & 0 & 0.86 \end{bmatrix}$	$\mathbf{Z}_{D_1} = \begin{bmatrix} 0.92 & 0 & 0.01 \\ 0 & 1.12 & 0 \\ 0 & 0 & 0.98 \end{bmatrix}$
$\mathbf{F}_2 = \begin{bmatrix} 1.14 & 0 & 0.47 \\ 0 & 0.95 & 0 \\ 0 & 0 & 0.94 \end{bmatrix}$	$\mathbf{Z}_{L_2} = \begin{bmatrix} 1.00 & 0 & 0.00 \\ 0 & 1.00 & 0 \\ 0 & 0 & 1.00 \end{bmatrix}$	$\mathbf{Z}_{D_2} = \begin{bmatrix} 1.05 & 0 & 0.03 \\ 0 & 0.94 & 0 \\ 0 & 0 & 0.99 \end{bmatrix}$
$\mathbf{F}_3 = \begin{bmatrix} 1.21 & 0 & 0.88 \\ 0 & 1.12 & 0 \\ 0 & 0 & 0.81 \end{bmatrix}$	$\mathbf{Z}_{L_3} = \begin{bmatrix} 1.06 & 0 & 0.41 \\ 0 & 1.18 & 0 \\ 0 & 0 & 0.86 \end{bmatrix}$	$\mathbf{Z}_{D_3} = \begin{bmatrix} 0.99 & 0 & -0.13 \\ 0 & 0.98 & 0 \\ 0 & 0 & 1.00 \end{bmatrix}$
$\mathbf{F}_4 = \begin{bmatrix} 1.21 & 0 & 0.77 \\ 0 & 1.09 & 0 \\ 0 & 0 & 0.78 \end{bmatrix}$	$\mathbf{Z}_{L_4} = \begin{bmatrix} 1.00 & 0 & -0.13 \\ 0 & 0.97 & 0 \\ 0 & 0 & 0.97 \end{bmatrix}$	$\mathbf{Z}_{D_4} = \begin{bmatrix} 1.58 & 0 & 0.40 \\ 0 & 1.25 & 0 \\ 0 & 0 & 0.53 \end{bmatrix}$
$\mathbf{F}_5 = \begin{bmatrix} 1.16 & 0 & 0.92 \\ 0 & 1.19 & 0 \\ 0 & 0 & 0.82 \end{bmatrix}$	$\mathbf{Z}_{L_5} = \begin{bmatrix} 0.96 & 0 & 0.23 \\ 0 & 1.09 & 0 \\ 0 & 0 & 1.05 \end{bmatrix}$	$\mathbf{Z}_{D_5} = \begin{bmatrix} 0.99 & 0 & -0.10 \\ 0 & 0.97 & 0 \\ 0 & 0 & 0.96 \end{bmatrix}$
$\mathbf{F}_6 = \begin{bmatrix} 1.15 & 0 & 0.77 \\ 0 & 1.15 & 0 \\ 0 & 0 & 0.79 \end{bmatrix}$	$\mathbf{Z}_{L_6} = \begin{bmatrix} 0.99 & 0 & -0.17 \\ 0 & 0.97 & 0 \\ 0 & 0 & 0.96 \end{bmatrix}$	$\mathbf{Z}_{D_6} = \begin{bmatrix} 0.96 & 0 & 0.09 \\ 0 & 1.09 & 0 \\ 0 & 0 & 1.05 \end{bmatrix}$
$\mathbf{F}_7 = \begin{bmatrix} 1.82 & 0 & 0.86 \\ 0 & 1.43 & 0 \\ 0 & 0 & 0.42 \end{bmatrix}$	$\mathbf{Z}_{L_7} = \begin{bmatrix} 1.58 & 0 & -0.45 \\ 0 & 1.25 & 0 \\ 0 & 0 & 0.53 \end{bmatrix}$	$\mathbf{Z}_{D_7} = \begin{bmatrix} 1.00 & 0 & -0.07 \\ 0 & 0.97 & 0 \\ 0 & 0 & 0.97 \end{bmatrix}$
$\mathbf{F}_8 = \begin{bmatrix} 1.81 & 0 & 0.63 \\ 0 & 1.40 & 0 \\ 0 & 0 & 0.42 \end{bmatrix}$	$\mathbf{Z}_{L_8} = \begin{bmatrix} 0.99 & 0 & -0.55 \\ 0 & 0.98 & 0 \\ 0 & 0 & 1 \end{bmatrix}$	$\mathbf{Z}_{D_8} = \begin{bmatrix} 1.06 & 0 & 0.42 \\ 0 & 1.18 & 0 \\ 0 & 0 & 0.86 \end{bmatrix}$
$\mathbf{F}_9 = \begin{bmatrix} 1.89 & 0 & 0.68 \\ 0 & 1.32 & 0 \\ 0 & 0 & 0.42 \end{bmatrix}$	$\mathbf{Z}_{L_9} = \begin{bmatrix} 1.05 & 0 & 0.05 \\ 0 & 0.94 & 0 \\ 0 & 0 & 0.99 \end{bmatrix}$	$\mathbf{Z}_{D_9} = \begin{bmatrix} 1.00 & 0 & 0.00 \\ 0 & 1.00 & 0 \\ 0 & 0 & 1.00 \end{bmatrix}$
$\mathbf{F}_{10} = \begin{bmatrix} 1.74 & 0 & 0.68 \\ 0 & 1.47 & 0 \\ 0 & 0 & 0.41 \end{bmatrix}$	$\mathbf{Z}_{L_{10}} = \begin{bmatrix} 0.92 & 0 & 0.14 \\ 0 & 1.12 & 0 \\ 0 & 0 & 0.98 \end{bmatrix}$	$\mathbf{Z}_{D_{10}} = \begin{bmatrix} 1.14 & 0 & 0.47 \\ 0 & 0.95 & 0 \\ 0 & 0 & 0.94 \end{bmatrix}$

References

Aoya, M., Wallis, S.R., 2003. Role of nappe boundaries in subduction-related regional deformation; spatial variation of meso- and microstructures in the Seba eclogite unit, the Sambagawa belt, SW Japan. Journal of Structural Geology 25, 1097–1106.

Bailey, C.M., Francis, B.E., Fahrney, E.E., 2004. Strain and vorticity analysis of transpressional high-strain zones from the Virginia Piedmont, U.S.A. In:

Alsop, G.I., Holdsworth, R.E., McCaffery, K.J.W., Hand, M. (Eds.), Flow Processes in Faults and Shear zones. Geological Society, London, Special Publications, vol. 234, pp. 249–264.

Bailey, C.M., Eyster, E.L., 2003. General shear deformation in the Pinaleño Mountains metamorphic core complex, Arizona. Journal of Structural Geology 25, 1883–1892.

Bhattacharyya, P., Hudleston, P., 2001. Strain in ductile shear zones in the Caledonides of northern Sweden: a three-dimensional puzzle. Journal of Structural Geology 23, 1549–1565.

Bobyarchick, A.R., 1986. The eigenvalues of steady flow in Mohr space. Tectonophysics 122, 35–51.

Brandon, M.T., 1995. Analysis of geologic strain data in strain-magnitude space. Journal of Structural Geology 17, 1375–1385.

Cobbold, P.R., 1976. Mechanical effects of anisotropy during large finite deformations. Bulletin de la Société Géologique de France 18, 1497–1510.

Cobbold, P.R., Cosgrove, J.W., Summers, J.M., 1971. Development of internal structures in deformed anisotropic rocks. Tectonophysics 12, 23–53.

Cutler, J.M., 1985. Error due to strain measurement in non-principal sections. Tectonophysics 113, 185–190.

Dunnet, D., Siddans, A.W.B., 1971. Nonrandom sedimentary fabrics and their modification by strain. Tectonophysics 12, 307–325.

Elliott, D., 1972. Deformation paths in structural geology. Geological Society of America Bulletin 83, 2621–2638.

Flinn, D., 1956. On the deformation of the Funzie conglomerate, Fetlar, Shetland. Journal of Geology 64, 480–505.

Flinn, D., 1961. On folding during three-dimensional progressive deformation. Journal of the Geological Society of London 118, 385–433.

Flinn, D., 1978. Construction and computation of three-dimensional progressive deformations. Journal of the Geological Society of London 135, 291–305.

Flinn, D., 1979. The deformation matrix and the deformation ellipsoid. Journal of Structural Geology 1, 299–307.

Fossen, H., Tikoff, B., 1997. Forward modeling of non-steady-state deformations and the "minimum strain path". Journal of Structural Geology 19, 987–996.

Furbish, D.J., 1997. Fluid Physics in Geology. Oxford UP, New York, 476 pp.

Giorgis, S., Markley, M., Tikoff, B., 2004. Vertical-axis rotation of rigid crustal blocks driven by mantle flow; vertical coupling and decoupling in the lithosphere. In: Grocott, J., McCaffrey, K.J.W., Taylor, G., Tikoff, B. (Eds.), Vertical Coupling and Decoupling in the Lithosphere. Geological Society, London, Special Publications, vol. 227, pp. 83–100.

Giorgis, S., Tikoff, B., McClelland, W., 2005. The missing Idaho arc: transpressional modification of the $^{87}Sr/^{86}Sr$ transition on the western edge of the Idaho batholith. Geology 33, 469–472.

Goodwin, L.B., Tikoff, B., 2002. Competency contrast, kinematics, and the development of foliations and lineations in the crust. Journal of Structural Geology 24, 1065–1085.

Goodwin, L.B., Williams, P.F., 1996. Deformation path partitioning within a transpressive shear zone, Marble Cove, Newfoundland. Journal of Structural Geology 18, 975–990.

Hansen, E., 1971. Strain Facies. Springer-Verlag, Berlin, 207 pp.

Holdsworth, R.E., Tavarnelli, E., Clegg, P., Pinheiro, R.V.L., Jones, R.R., McCaffrey, K.J.W., 2002. Domainal deformation patterns and strain partitioning during transpression: an example from the Southern Uplands terrane, Scotland. Journal of the Geological Society 159, 401–415.

Horsman, E., Tikoff, B., 2005. Quantifying simultaneous discrete and distributed deformation. Journal of Structural Geology 27, 1168–1189.

Hossack, J.R., 1968. Pebble deformation and thrusting in the Bygdin area (southern Norway). Tectonophysics 5, 315–339.

Hsu, T.C., 1966. The characteristics of coaxial and non-coaxial strain paths. Journal of Strain Analysis 1, 216–222.

Hull, J., 1988. Thickness–displacement relationships for deformation zones. Journal of Structural Geology 10, 431–435.

Ishii, K., 1992. Partitioning of non-coaxiality in deforming layered rock masses. Tectonophysics 210, 33–43.

Jiang, D., 1994. Vorticity determination, distribution, partitioning and the heterogeneity and non-steadiness of natural deformations. Journal of Structural Geology 16, 121–130.

Jiang, D., White, J.C., 1995. Kinematics of rock flow and the interpretation of geological structures, with particular reference to shear zones. Journal of Structural Geology 17, 1249–1265.

Jiang, D., Williams, P.F., 1998. High-strain zones: a unified model. Journal of Structural Geology 20, 1105–1120.

Jones, R.R., Holdsworth, R.E., Bailey, W., 1997. Lateral extrusion in transpression zones: the importance of boundary conditions. Journal of Structural Geology 19, 1201–1217.

Jones, R.R., Tanner, P.W.G., 1995. Strain partitioning in transpression zones. Journal of Structural Geology 17, 793–802.

Lin, S., Jiang, D., Williams, P.F., Holdsworth, R.E., Strachan, R.A., Dewey, J.F., 1998. Transpression (or transtension) zones of triclinic symmetry: natural example and theoretical modelling. In: Continental Transpression and Transtension Tectonics. Geological Society, London, Special Publications, vol. 135, pp. 41–57.

Lisle, R.J., 1977. Estimation of the tectonic strain ratio from the mean shape of deformed elliptical markers. Geologie en Mijnbouw 56, 140–144.

Lisle, R.J., 1979. Strain analysis using deformed pebbles; the influence of initial pebble shape. Tectonophysics 60, 263–277.

Lisle, R.J., 1985. Geological strain analysis: a manual for the R_f/ϕ technique. Pergamon, Oxford, 95 pp.

Lisle, R.J., Rodeel, H.E., Doorn, D., Brugge, J., van de Gaag, P., 1983. Estimation of viscosity contrast and finite strain from deformed elliptical inclusions. Journal of Structural Geology 5, 603–609.

Lister, G.S., Williams, P.F., 1983. The partitioning of deformation in flowing rock masses. Tectonophysics 92, 1–33.

MacInnes, E.A., White, J.C., 2004. Geometric and kinematic analysis of a transpression terrane boundary: Minas fault system, Nova Scotia, Canada. In: Alsop, G.I., Holdsworth, R.E., McCaffrey, K.J.W., Hand, M. (Eds.), Flow Processes in Faults and Shear Zones. Geological Society, London, Special Publications, vol. 224, pp. 201–214.

Malvern, L.E., 1969. An Introduction to the Mechanics of a Continuous Medium. Prentice-Hall, Englewood Cliffs, NJ, 713 pp.

Means, W.D., 1976. Stress and Strain. Springer-Verlag, New York, 339 pp.

Means, W.D., 1994. Rotational quantities in homogeneous flow and the development of small-scale structure. Journal of Structural Geology 16, 437–445.

Means, W.D., Lister, G.S., Williams, P.F., 1980. Vorticity and non-coaxiality in progressive deformations. Journal of Structural Geology 2, 371–378.

Means, W.D., 1984. Shear zones of types I and II and their significance for reconstruction of rock historyAbstracts with Programs (Northeast Section Meeting). Geological Society of America 16, 50.

Means, W.D., 1995. Shear zones and rock history. Tectonophysics 247, 157–160.

Mitra, G., 1991. Deformation of granitic basement rocks along fault zones at shallow to intermediate crustal levels. In: Mitra, S., Fisher, G.W. (Eds.), Structural Geology of Fold and Thrust Belts. Johns Hopkins UP, Baltimore, pp. 123–144.

Montesi, L.G.J., Hirth, G., 2003. Grain size evolution and the rheology of ductile shear zones: from laboratory experiments to postseismic creep. Earth and Planetary Science Letters 211, 97–110.

Nadai, A., 1963. Theory of Flow and Fracture of Solids, vol. 2. McGraw-Hill, New York, 705 pp.

Owens, W.H., 1974. Representation of finite strain state by three-axis planar diagrams. Geological Society of America Bulletin 85, 307–310.

Passchier, C.W., 1986. Flow in natural shear zones – the consequences of spinning flow regimes. Earth and Planetary Science Letters 77, 70–80.

Passchier, C.W., 1988. Analysis of deformation paths in shear zones. Geologische Rundschau 77, 309–318.

Piazolo, S., Passchier, C.W., 2002. Controls on lineation development in low to medium grade shear zones; a study from the Cap de Creus peninsula, NE Spain. Journal of Structural Geology 24, 25–44.

Provost, A., Buisson, C. and Merle, O., 2004. From progressive to finite deformation and back. Journal of Geophysical Research: Solid Earth and Planets 109, B02405.

Ramberg, H., 1975. Particle paths, displacement and progressive strain applicable to rocks. Tectonophysics 28, 1–37.

Ramsay, J.G., 1967. Folding and Fracturing of Rocks. McGraw-Hill, New York, 568 pp.

Ramsay, J.G., 1980. Shear zone geometry; a review; shear zones in rocks. Journal of Structural Geology 2, 83–99.

Ramsay, J.G., Allison, I., 1979. Structural analysis of shear zones in an alpinised Hercynian granite (Maggia Lappen, Pennine zone, central Alps). Swiss Bulletin of Mineralogy and Petrology 59, 251–279.

Ramsay, J.G., Graham, R.H., 1970. Strain variation in shear belts. Canadian Journal of Earth Sciences 7, 786–813.

Robin, P.Y.F., Cruden, A.R., 1994. Strain and vorticity patterns in ideally ductile transpression zones. Journal of Structural Geology 16, 447–466.

Schultz-Ela, D.D., 1990. A method for estimating errors in calculated strains. Journal of Structural Geology 12, 939–943.

Simpson, C., 1985. Deformation of granitic rocks across the brittle–ductile transition. Journal of Structural Geology 7, 503–511.

Simpson, C., DePaor, D.G., 1993. Strain and kinematic analysis in general shear zones. Journal of Structural Geology 15, 1–20.

Tikoff, B., Fossen, H., 1993. Simultaneous pure and simple shear – the unifying deformation matrix. Tectonophysics 217, 267–283.

Tikoff, B., Fossen, H., 1995. The limitations of 3-dimensional kinematic vorticity analysis. Journal of Structural Geology 17, 1771–1784.

Tikoff, B., Fossen, H., 1999. Three-dimensional reference deformations and strain facies. Journal of Structural Geology 21, 1497–1512.

Tikoff, B., Teyssier, C., 1994. Strain modeling of displacement-field partitioning in transpression orogens. Journal of Structural Geology 16, 1575–1588.

Treagus, S.H., 1988. Strain refraction in layered systems. Journal of Structural Geology 10, 517–527.

Treagus, S.H., 1993. Flow variations in power-law multilayers – implications for competence contrasts in rocks. Journal of Structural Geology 15, 423–434.

Treagus, S.H., Cobbold, P.R., Schwerdtner, W.M., 1983. A theory of finite strain variation through contrasting layers, and its bearing on cleavage refraction; strain patterns in rocks. Journal of Structural Geology 5, 351–368.

Truesdell, C., 1954. The Kinematics of Vorticity. Indiana UP, Bloomington, 232 pp.

Turner, F.J., Weiss, L.E., 1963. Structural Analysis of Metamorphics Tectonites. McGraw-Hill, New York, 545 pp.

Weijermars, R., 1992. Progressive deformation in anisotropic rocks. Journal of Structural Geology 14, 723–742.

West Jr., D.P., Hubbard, M.S., 1997. Progressive localization of deformation during exhumation of a major strike-slip shear zone: Norumbega fault zone, south-central Maine, USA. Tectonophysics 273, 185–201.

Wheeler, J., 1986. Strain analysis in rocks with pretectonic fabrics. Journal of Structural Geology 8, 887–896.

White, S.H., Burrows, S.E., Carreras, J., Shaw, N.D., Humphreys, F.J., 1980. On mylonites in ductile shear zones. Journal of Structural Geology 2, 175–187.

Wojtal, S., Mitra, G., 1988. Nature of deformation in some fault rocks from Appalachian thrusts. In: Mitra, G., Wojtal, S. (Eds.), Geometries and Mechanisms of Thrusting, with Special Reference to the Appalachians. Geological Society of America Special Paper 222, pp. 17–33.

Yamaji, A., 2005. Finite tectonic strain and its error, as estimated from elliptical objects with a class of initial preferred orientations. Journal of Structural Geology 27, 2030–2042.

Zhang, G., Hynes, A., 1995. Determination of position gradient tensor from strain-measurements and its implications for the displacement across a shear zone. Journal of Structural Geology 17, 1587–1599.